

Unclassified

SECURITY CLASSIFICATION OF THIS PAGE (When Data Entered)

20000801181

②

REPORT DOCUMENTATION PAGE		READ INSTRUCTIONS BEFORE COMPLETING FORM
1. REPORT NUMBER ARO 19979.3-EG	2. GOVT ACCESSION NO. <b>AD-A161 756</b>	3. RECIPIENT'S CATALOG NUMBER
4. TITLE (and Subtitle) A Study of Singularities in Boundary-Fitted Coordinate Systems		5. TYPE OF REPORT & PERIOD COVERED Final Report 16 Aug 83 - 15 Aug 85
7. AUTHOR(s) Helen V. McConnaughey		6. PERFORMING ORG. REPORT NUMBER
9. PERFORMING ORGANIZATION NAME AND ADDRESS Mississippi State Univ. Mississippi State, MS 39762		8. CONTRACT OR GRANT NUMBER(s) DAAG29-83-K-0101
11. CONTROLLING OFFICE NAME AND ADDRESS U. S. Army Research Office Post Office Box 12211 Research Triangle Park, NC 27709		10. PROGRAM ELEMENT, PROJECT, TASK AREA & WORK UNIT NUMBERS N/A
14. MONITORING AGENCY NAME & ADDRESS (if different from Controlling Office)		12. REPORT DATE October 9, 1985
		13. NUMBER OF PAGES 42
		15. SECURITY CLASS. (of this report) Unclassified
16. DISTRIBUTION STATEMENT (of this Report) Approved for public release; distribution unlimited.		15a. DECLASSIFICATION/DOWNGRADING SCHEDULE
17. DISTRIBUTION STATEMENT (of the abstract entered in Block 20, if different from Report)		
18. SUPPLEMENTARY NOTES The view, opinions, and/or findings contained in this report are those of the author(s) and should not be construed as an official Department of the Army position, policy, or decision, unless so designated by other documentation		
19. KEY WORDS (Continue on reverse side if necessary and identify by block number) Coordinate Systems      Two-Dimensional Configurations Boundary-Fitted Coordinate Systems      Three-Dimensional Grids Subsystems      Grid Structures		
20. ABSTRACT (Continue on reverse side if necessary and identify by block number) Studies have indicated that special points encountered in a finite-difference approach must be individually examined before a suitable treatment of each can be identified. In a finite-volume formulation, however, the same treatment applies to all special cells.		

DTIC  
ELECTE  
NOV 26 1985

E

AD-A161 756

DTIC FILE COPY

Reproduced From  
Best Available Copy

DD FORM 1 JAN 73 1473

EDITION OF 1 NOV 65 IS OBSOLETE

UNCLASSIFIED

85 11 18 14

Final Report

ARO Contract No. DAAG 29-83-K-0101

A STUDY OF SINGULARITIES IN  
BOUNDARY-FITTED COORDINATE SYSTEMS

by

Dr. Helen V. McConnaughey  
Department of Mathematics  
Mississippi State University  
Mississippi State, MS 39762

469108

October 9, 1985

## **REPRODUCTION QUALITY NOTICE**

**This document is the best quality available. The copy furnished to DTIC contained pages that may have the following quality problems:**

- **Pages smaller or larger than normal.**
- **Pages with background color or light colored printing.**
- **Pages with small type or poor printing; and or**
- **Pages with continuous tone material or color photographs.**

**Due to various output media available these conditions may or may not cause poor legibility in the microfiche or hardcopy output you receive.**

☐

**If this block is checked, the copy furnished to DTIC contained pages with color printing, that when reproduced in Black and White, may change detail of the original copy.**

# TABLE OF CONTENTS

Introduction	1
Project Results	2
Conclusion	4
References	5
Figures	6
Appendix 1	
Appendix 2	

Accession For	
NTIS GRA&I	<input checked="" type="checkbox"/>
DTIC TAB	<input type="checkbox"/>
Unannounced	<input type="checkbox"/>
Justification	
By _____	
Distribution/	
Availability Codes	
Dist	Avail and/or Special
A-1	



## INTRODUCTION

Many problems in science and engineering require the solution of a system of partial differential equations on a complex two- or three-dimensional domain. In order to solve such a problem numerically, a boundary-fitted coordinate system is usually constructed. For geometries of practical importance, it is often necessary to partition the domain and to fit a separate coordinate system to each subregion. Patching these subsystems together to form a composite system can produce irregular grid structures where the numerical scheme of solution must be modified.

Methods for treating nonstandard ("special") grid points in two-dimensional configurations were developed and reported earlier in the course of this project. (See Ref. 1-3). Verification of these methods through computer experimentation and extension of the methods to special points in three-dimensional grids were the primary objectives of the project reported here. *K. J. ...*

## PROJECT RESULTS

The same general approach used to develop and analyze methods for treatment of special two-dimensional grid structures was applied to three-dimensional configurations. The characterization of special points in three dimensions is a direct and straightforward extension of that reported for two-dimensional geometries (Ref. 1). Ordinary three-dimensional grid structures are depicted in Fig. 1 and 2. Such structures may not exist at some boundary points or where two or more subregions of a composite grid meet. Examples are shown in Fig. 3 and 4. These nonstandard grid structures require an adjustment of numerical solution schemes which are based on the usual grid-point orientation shown in Fig. 1 and 2.

As in the case of two-dimensional geometries, a finite-difference scheme can be applied at a special point in three dimensions if the scheme is rephrased in terms of a suitable local coordinate system. This local system must have an ordinary structure (as in Fig. 1 or 2) and should not be too stretched or skewed. The appropriate local coordinate systems for the special points in Fig. 3 and 4 are illustrated in Fig. 5 and 6. It should be noted that for some configurations, a satisfactory local coordinate system may not exist. An example is shown in Fig. 7. In such cases, a finite-volume approach must be used to approximate derivatives at the special point.

Irregular grid structures can generally be treated in a simple and straightforward manner when a finite-volume approach is used. Then, it is the configuration of grid cells which is at issue. Extension of the two-dimensional analysis of Ref. 1-3 shows a special cell in three

dimensions to have other than six faces or a vertex common to other than eight cells. The latter type of special cell requires special attention only when a derivative must be represented on a cell face.

In direct analogy to the approach for two dimensions detailed in Ref. 2 and 3 (attached herewith), special cells are treated by imposing the integral form of the governing equations in physical coordinates, rather than in terms of the transformed (curvilinear) coordinates, within the special volume element. Cell-centered values of the unknown functions are sought. A derivative within the cell is approximated by a surface integral over the cell boundary which is equivalent to the average of that derivative over the cell. In particular, identity (1) is used:

$$\bar{\nabla} f_{\text{avg}} = \frac{1}{V} \int_D \nabla f \, d\tau = \frac{1}{V} \int_{\partial D} f \, \underline{n} \, d\sigma, \quad (1)$$

where  $V$  is the volume of cell  $D$ ,  $d\tau$  is an increment of volume,  $\partial D$  is the surface bounding cell  $D$ , and  $\underline{n}$  is the unit outward normal to surface-area element  $d\sigma$ . The value of the unknown function,  $f$ , on a cell face is equated to an average of the function's values at the centers of the cells sharing that face. The value of a derivative, e.g.  $\frac{\partial f}{\partial x}$ , on a cell face is equated to the average of the derivative's values at the vertices of that cell face. These vertex values are obtained by applying identity (1) to an auxiliary cell centered at each vertex. The cumbersome formulas for these expressions in three dimensions are omitted here, but they can be derived by directly extending the formulas for two-dimensional cells given in Ref. 2.

#### CONCLUSION

The previous discussion shows that special points encountered in a finite-difference approach must be individually examined before a suitable treatment of each can be identified. In a finite-volume formulation, however, the same treatment applies to all special cells. Also, from a finite-volume point of view, fewer grid structures are "special" than from a finite-difference perspective. Thus, in most cases involving irregular grid structures, a finite-volume formulation of the problem at the special points is recommended.

#### REFERENCES

1. McDonnaughey, H.V. and Thompson, J.F. "A Study of Singularities in Boundary-Fitted Coordinate Systems", Renewal proposal for ARC Contract No. DAA3-78-83-X-0101, 1981.
2. Mastin, C.W. and McDonnaughey, H.V. "Computational Problems on Composite Grids", AIAA Paper No. AIAA-84-1611, AIAA 17th Fluid and Plasma Dynamics Conference, Snowmass, Colorado, 1984.
3. McDonnaughey, H.V. "Numerical Implementation", Chapter IV of Numerical Grid Generation: Foundations and Applications (J.F. Thompson, E.O.A. Warsi, C.W. Mastin, auth.), North-Holland, 1985.

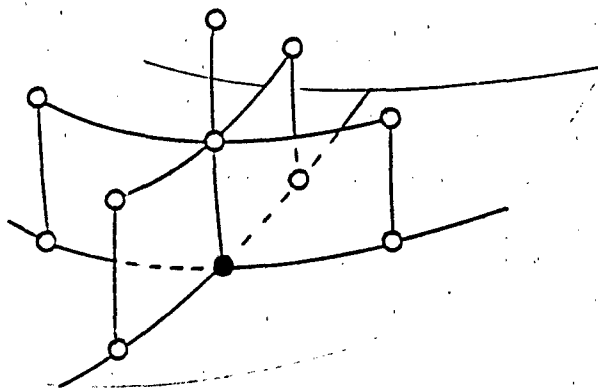


Figure 1

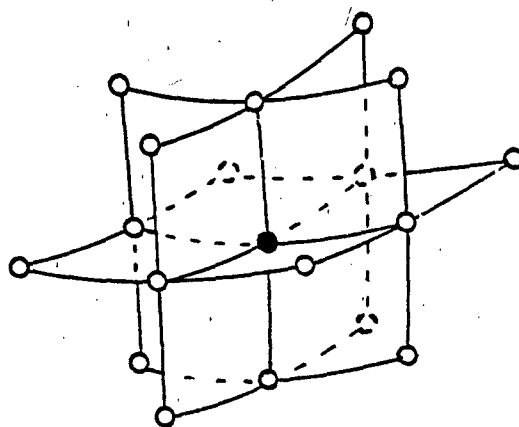


Figure 2

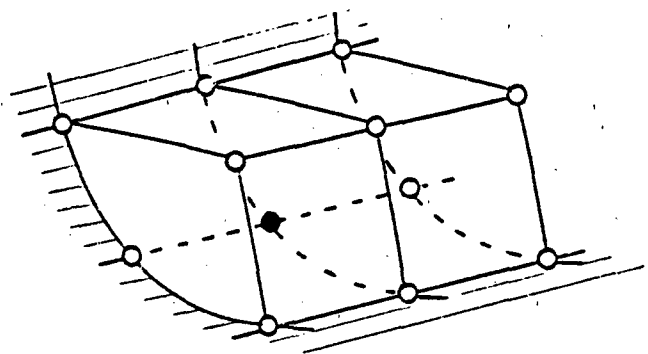


Figure 3

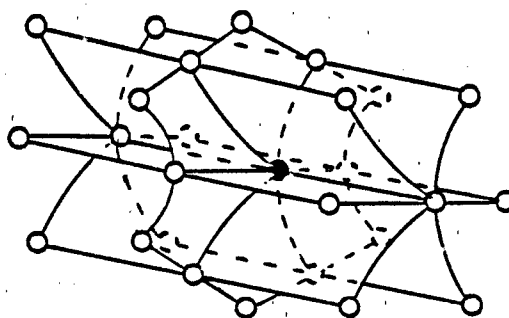


Figure 4

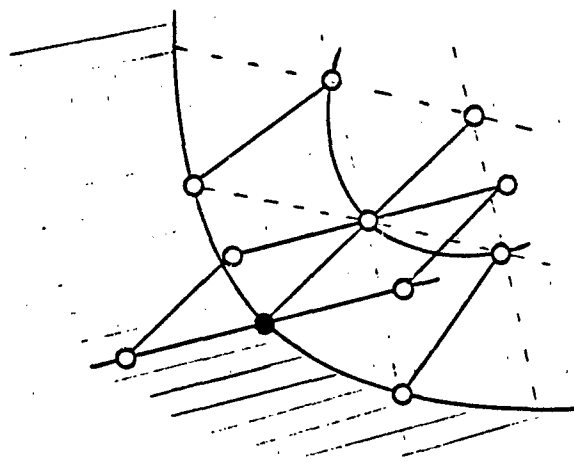


Figure 5

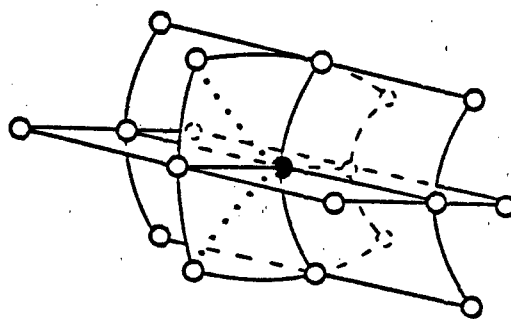


Figure 6

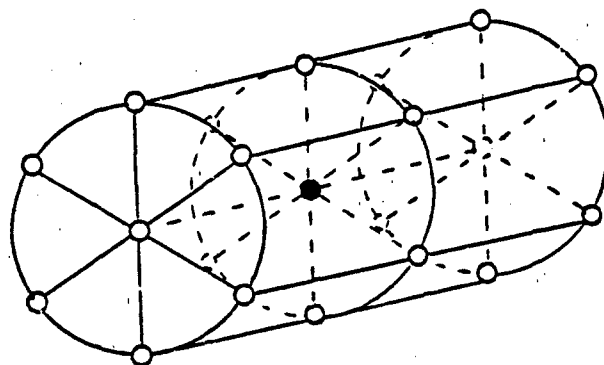


Figure 7

APPENDIX 1

Reference 2

Computational Problems on Composite Grids

by

C.W. Mastin and H.V. McConnaughey

AIAA Paper No. AIAA-84-1611

AIAA 17th Fluid and Plasma Dynamics Conference

Snowmass, Colorado, 1984

AIAA-84-1611  
COMPUTATIONAL PROBLEMS  
ON COMPOSITE GRIDS\*

C. Wayne Mastin and H. V. McConnaughey  
Mississippi State University  
Mississippi State, MS 39762

Abstract

Complex physical regions often necessitate the use of several rectangular computational regions. The corresponding physical subregions may be joined along their boundary or overlapped. Techniques are described for the numerical solution of partial differential equations on either type of composite grid system.

Introduction

Problems in constructing a computational grid often arise due to the complex geometric configurations encountered in practical fluid flow simulations. For example, an aircraft is composed of many individual components such as fuselage, wings, tail, fins, pylons, and nacelles. Although each component may be geometrically simple, and a grid about the individual components may be easy to construct, constructing a grid about the complete configuration is more difficult. Another example in which complex regions are encountered may be found by examining the design of current turbomachinery. The problem of constructing a grid is compounded by the accuracy requirements of the numerical algorithm. In order to control the truncation error of the algorithm, grid points must be concentrated near boundary layers, shocks, and other regions where solution gradients are large. It is thus apparent that where a boundary-fitted curvilinear coordinate system is employed in the solution of many problems of practical interest, several rectangular computational regions must be used. The grid which is defined by this merging of several coordinate systems is called a composite grid.

Two approaches have developed in constructing composite grid systems. The first, and still the most popular, is to have the grid lines pass smoothly from one subregion into the next.<sup>1,2</sup> The well-known chain rule formulas can be used to transform from the physical to the computational variables at the interior points of each subregion as well as at points

lying along the sides of two subregions. However the vertices present a problem whenever the Jacobian of the transformation is zero or is undefined. This same problem may also occur at boundary points of the physical region. One of the objectives of this report is to classify the types of singular or unusual points which may occur and indicate how to derive consistent difference approximations at such points. The second approach in working with composite grids is to overlap the grids for the physical subregions. In this case the solution values are transferred from the interior points of one grid to the boundary points of another grid by an interpolation formula. Many different interpolation schemes are available and their effect on the error in the numerical solution may be significant. Overlapping grids have been gaining in popularity due to the inherent freedom in generating each subregion grid without consideration of the remaining grids.

Computational techniques and comparative results on composite grids will be presented in the solution of simple two-dimensional model problems. In the case where grid lines continue smoothly between subregions, a finite-volume method is compared with an ADI scheme using the usual finite-difference approximations. The first method illustrates the use of finite-volume formulations for solving partial differential equations with second-order derivatives, while the second demonstrates an implementation of ADI schemes on composite grids with singular points. Solutions are also presented from computations on overlapping grids. The questions to be discussed there are: What effect does the interpolation procedure have on the accuracy of the numerical solution? How does the accuracy vary with the choice of the particular interpolation formula? Specifically, comparisons are presented using bivariate interpolation on quadrilaterals<sup>3,4</sup>, Taylor polynomials<sup>5</sup>, and the triangular interpolation schemes commonly used with finite element methods.

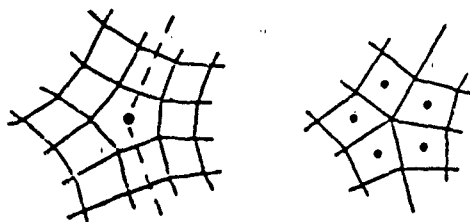
Special Points in Continuous Grids

Field points which require special attention frequently arise when numerically solving flow problems on a composite curvilinear coordinate system consisting of continuously joined segments. This is true whether the numerical method of solution involves a finite-volume formulation or

\*This work was supported by the Army Research Office under Grant DAAG 29-83-K-0101 and by NASA Langley Research Center under Grant NSG-1577.

a finite-difference scheme. The special points encountered in the two approaches are, however, different in nature, hence the two cases are addressed separately in the following discussion.

In a finite-volume scheme on a two-dimensional composite grid, the unusual points which arise are centers of interior grid cells having other than four edges or having a vertex shared by other than four cells. Examples are illustrated below.



The first type of cell can result when sub-regions of the segmented domain are joined between grid lines; the second can occur when segments are joined along grid lines, but this cell requires special care only when second derivatives are approximated therein. In either case, treatment of the associated "special points" consists simply of replacing the usual difference representations associated with four-sided cells having vertices common to three other cells by expressions derived for a general N-sided cell.

Recall that a finite-volume formulation solves for cell-centered function values and approximates derivatives at a cell center by line integrals about the cell boundary which are equivalent to averages over the cell. In particular, identity (1) is used.

$$\int_D \nabla f \cdot d\mathbf{s} = \int_{\partial D} f \mathbf{n} \cdot d\mathbf{s} \quad (1)$$

For an N-sided cell of area A with cartesian centroid  $P = (p_1, p_2)$ , vertices  $V^i = (v_1^i, v_2^i)$   $i = 1, 2, \dots, N$ , and edges  $s^i$  joining  $V^i$  and  $V^{i+1}$  ( $V^{N+1} = V^1$ ) along which a function  $f$  and its first partial derivatives are constant, this approach gives

$$\begin{aligned} f_x^P &= A^{-1} \sum_{i=1}^N f^{s^i} (v_2^{i+1} - v_2^i) \\ f_y^P &= A^{-1} \sum_{i=1}^N f^{s^i} (v_1^i - v_1^{i+1}) \\ f_{xx}^P &= A^{-1} \sum_{i=1}^N f_x^{s^i} (v_2^{i+1} - v_2^i) \\ f_{yy}^P &= A^{-1} \sum_{i=1}^N f_y^{s^i} (v_1^i - v_1^{i+1}) \end{aligned} \quad (2)$$

where the superscripts on  $f$  and its derivatives indicate the point or face of evaluation.

Simple forward/backward differencing can be used to approximate edge values

$f^{s^i}$ ,  $f_x^{s^i}$ , and  $f_y^{s^i}$  when working on a grid whose

interior is "rectangular" in nature in that right/left and up/down orientations can be followed through the grid in an unambiguous way. Such a technique was used in the numerical example discussed later. On a more general grid, an obvious way to approximate

$f^{s^i}$  is to average the center values of the two cells sharing edge  $s^i$ . This same averaging scheme cannot be repeated to approximate

$f_x^{s^i}$ , and  $f_y^{s^i}$ , however, without rejecting the

customary strategy of avoiding use of values at points which are not immediate neighbors of the point at which a quantity is being evaluated. Instead, we propose the averaging technique:

$$\begin{aligned} f_x^{s^i} &= \frac{1}{2} (f_x^{V^i} + f_x^{V^{i+1}}) \\ f_y^{s^i} &= \frac{1}{2} (f_y^{V^i} + f_y^{V^{i+1}}) \end{aligned} \quad (3)$$

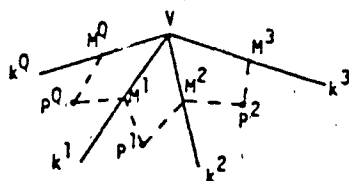
where the vertex values are obtained by applying identity (1) to auxiliary cells formed by joining the midpoints of the edges of each cell to the cell center. To make this more precise, let  $V$  be a vertex common to  $Q$  cells and label the cell faces emanating from  $V$  as  $k^i$  with midpoints

$M^i = (m_1^i, m_2^i)$   $i = 1, 2, \dots, Q$ . Then, if  $P^i =$

$(p_1^i, p_2^i)$  is the center of the cell having edges  $k^i$  and  $k^{i+1}$ , and if  $f$  is taken to equal  $f^{P^i}$  along  $M^i$  and  $M^{i+1}$ , the first partial derivatives of  $f$  at  $V$  may be approximated by

$$\begin{aligned} f_x^V &= A^{-1} \sum_{i=1}^Q f^{P^i} (m_2^{i+1} - m_2^i) \\ f_y^V &= A^{-1} \sum_{i=1}^Q f^{P^i} (m_1^i - m_1^{i+1}) \end{aligned} \quad (4)$$

where  $A$  is the area of the  $2Q$ -faced auxiliary cell  $M^1 P^1 M^2 P^2 \dots M^Q P^Q M^1$  indicated in the following diagram.

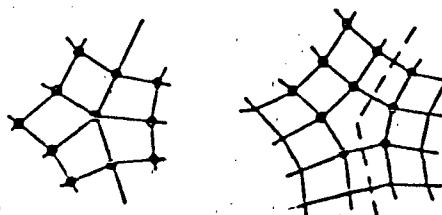


Expressions (3), (4), and the average

$$r^{k1} = \frac{1}{2} (r^{p1-1} + r^{p1})$$

make the difference formulas in (2) reasonable approximations of the first and second partial derivatives of a function  $f$  at the center of an arbitrary grid cell. Because this technique is generally applicable, the finite-volume approach is deemed the most straight-forward when special points are present in the field. In the alternative finite-difference approach, it is found that special points which arise must be individually examined before a suitable treatment of each can be identified. Thus no single set of finite-difference formulas can always be applied to every such point independent of its context, as will now be discussed.

The special points which are encountered in a finite-difference formulation may be recognized as those grid points (cell vertices) having a nonstandard number of immediate neighbors. On the boundary of a two-dimensional domain, such points have other than five neighbors but require special treatment only if Neumann boundary conditions are imposed. Interior grid points are "special" if they have other than eight immediate neighbors. These can occur on the interface between segments of a composite grid which are joined along grid lines, or they can be vertices of a cell intersected by an interface in the case of subregions joined between grid lines (see below).



In all cases, the usual finite-difference approach can be followed if the difference formulas are rephrased in terms of suitable local coordinates which identify and label the standard number of neighbors. Thompson<sup>6</sup> has described such local systems for special boundary points; choices appropriate to various interior special points are indicated in Figure 1.

The usual transformation relations applied to the local coordinates  $(\xi, \eta)$  at a special point  $P$  provide accurate difference approximations of derivatives with respect to the physical variables there. This technique was applied to the special boundary point shown in Figure 2 when the associated partial differential equation was numerically solved using a finite-difference scheme.

### Overlapping Grids

When overlapping grids are constructed, any boundary point of a component grid  $G$ , which is not a physical boundary point, must lie in a cell of some grid  $H$ . Regardless of the difference equations or the algorithm used to solve the difference equations, there must be a transmission of information between the various grid systems. Suppose that solution values on  $H$  are transmitted to the grid  $G$  by a general interpolation formula

$$f(r_0) = \sum_{j=1}^k a_j f(s_j) \quad (5)$$

where  $r_0$  is a boundary point of  $G$  and the  $s_j$  are points of  $H$ . At least some of the  $s_j$  must be interior points of  $H$  and, depending on the algorithm, one may wish to require a sufficiently large overlapping so that all the  $s_j$  are interior points. For example, the latter requirement would eliminate possible stability problems when solving parabolic equations. When the value of  $f$  at  $r_0$  is replaced in the difference equation at a neighboring point by the interpolated value, a new difference equation results which will have a different local truncation error. It can be shown that a sufficient condition for consistency in the approximation of the first-order derivatives with respect to the physical variables  $x$  and  $y$  is that

$$\sum_{j=1}^k a_j = 1, \quad \sum_{j=1}^k a_j x_j = x_0, \quad \sum_{j=1}^k a_j y_j = y_0 \quad (6)$$

where  $x_0$  and  $y_0$  denote the coordinates of  $r_0$ , and  $x_j$  and  $y_j$  denote the coordinates of  $s_j$ . The difference approximations will be second-order accurate if in addition

$$\sum_{j=1}^k a_j x_j^2 = x_0^2, \quad \sum_{j=1}^k a_j x_j y_j = x_0 y_0, \quad \sum_{j=1}^k a_j y_j^2 = y_0^2 \quad (7)$$

There is a loss of one order in the formal accuracy of the second-order derivative approximations.

Several different interpolation schemes will now be reviewed. The first scheme is based on the approximation of a Taylor polynomial. For each boundary point  $r_0$  of  $G$ , find the closest point  $s_1$  of  $H$ . The values of the function  $f$  at the four neighbors of  $s_1$ , say  $s_2, \dots, s_5$ , can be used to calculate approximations of the first derivatives of the actual solution. These approximations can thus be substituted for the derivatives in a linear Taylor polynomial at  $s_1$ . If the resulting interpolation formula is written in the form of (5), then the coefficients will satisfy (6). If the original algorithm is at least second order accurate, then there is no loss of accuracy in replacing the derivatives by differences. Therefore, the use of this interpolation formula would give consistent approximations of first derivatives. Clearly, one could also construct an approximation of a quadratic Taylor polynomial. However, the consistency of the second derivative approximations cannot be guaranteed unless the local truncation error in the finite-difference equations exceeds two. Therefore, if a second-order algorithm is being implemented, it is not clear that a quadratic polynomial would give better results than a linear polynomial.

The next interpolation formula does not require the numerical approximation of derivatives. Let  $r_0$  belong to a grid cell  $C$  of  $H$  with vertices  $s_1, \dots, s_4$ . There exists a unique bilinear mapping of the unit square onto the cell  $C$ . The point  $r_0$  must be the image of some point in the unit square so that

$$r_0 = (1-u)(1-v)s_1 + u(1-v)s_2 + v(1-u)s_4 + uv s_3$$

for  $0 \leq u, v \leq 1$ . Since the coordinates of all points are known, this system can be solved explicitly for  $u$  and  $v$ . If  $f$  is also assumed to be a bilinear function of  $u$  and  $v$ , then

$$f(r_0) = (1-u)(1-v)f(s_1) + u(1-v)f(s_2) + v(1-u)f(s_4) + uvf(s_3). \quad (8)$$

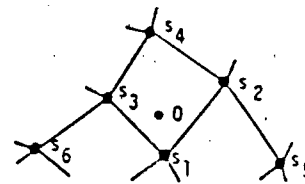
This interpolation formula satisfies (6). This scheme can also be generalized to construct interpolation formulas of arbitrary order. The procedure for biquadratic interpolation will be briefly described. Let  $Q$  be the union of four grid cells containing  $r_0$ . There exists a unique biquadratic mapping of the unit square such that the points  $(u, v)$  where  $u=0, 1/2, 1, v=0, 1/2, 1$ , map to the vertices of  $Q$ . Now the coordinates of the point in the unit square which has  $r_0$  as its image can be found by solving a system of two biquadratic equations. Unfortunately, these equations would be difficult to solve directly. In the examples which follow, these equations were solved numerically using Newton's iteration method. Once the

approximate values of  $u$  and  $v$  have been calculated, a biquadratic interpolant of the following form is computed.

$$f(r_0) = \sum_{j=1}^9 q_j(u, v)f(s_j) \quad (9)$$

Here  $q_j$  is the biquadratic Lagrange interpolating polynomial which assumes the value 1 at the point of the unit square which maps to  $s_j$  and vanishes at the points which have other grid points of  $Q$  as images. This interpolation formula satisfies both (6) and (7). Thus, improved results would be anticipated using biquadratic interpolation. It should be noted that the above interpolating functions are bilinear and biquadratic functions of the variables  $u$  and  $v$  which are sometimes referred to as isoparametric coordinates. Bilinear and higher-order interpolation on the physical variables  $x$  and  $y$  is generally not feasible unless the cell sides are aligned with the coordinate axes.

Partly due to the need for an iterative method in determining the interpolation coefficients, it was decided that interpolation on triangular regions would be investigated. Such interpolation is popular in finite-element analysis, and it can be readily adapted to the present problem. If  $r_0$  belongs to a grid cell  $C$ , then either diagonal of  $C$  determines a triangular region containing  $r_0$ . Select one of these triangular regions and let its vertices be denoted as  $s_1, s_2, s_3$ . In this case, the three equations in (6) determine the coefficients  $a_j$  of the linear interpolating formula (5). This is referred to as linear interpolation since it is equivalent to interpolating by a linear function of  $x$  and  $y$  with values given at  $s_1, s_2$ , and  $s_3$ . A quadratic interpolation can be constructed from three points at the vertices of a triangular region and three points along the sides. Such a configuration arises if the grid points of  $H$  are selected as in this figure.



Again the coefficients of the interpolation formula are solutions of a linear system of equations, namely, the equations in (6) and (7). Then the interpolated value is obtained by using these coefficients in (5).

So far only accuracy considerations have been investigated. When solving elliptic and parabolic equations, iterative convergence and stability are also of interest. If only the interpolation formula (5) is considered, convergence and stability would be guaranteed if

the coefficients are non-negative. This would therefore be a desirable condition although certainly not necessary. The linear and bilinear are the only interpolation formulas with non-negative coefficients. It can also be noted that the convergence or stability of the finite-difference algorithm would be least affected if there were sufficient overlap of grids so that all the  $s_i$  are interior grid points of  $H$ . This is because all the  $f(s_i)$  values would be updated when the interpolation procedure was implemented.

#### Computational Examples

The problems considered here are, for the most part, simple model problems where an exact solution is known. Hence, the accuracy of the various techniques discussed in the previous sections can be compared. The physical regions are also quite simple, but they do exhibit the computational problems inherent in more complex configurations.

The advantages of the cell-centered finite volume method in the solution of problems on regions with special points has already been discussed. Recent literature contains many applications of the method to the solution of hyperbolic conservation laws. In the case of four-sided cells, the method can also be applied in a straightforward manner to the solution of parabolic and elliptic equations by using the forward/backward differences which were mentioned earlier. A second-order approximation is obtained by switching the direction of differencing in the two difference operations which must be applied to generate an approximation of a second-order derivative. In the results of this report, the four possible difference quotients obtained by all combinations of forward and backward differencing have been averaged to yield a second-order difference expression which would also reflect any symmetry in the grid. It was observed that considerable simplification in imposing boundary conditions resulted if only two of the difference expressions were averaged at the boundary. If Neumann boundary conditions were specified, differencing in the direction exterior to the region was performed only in the second application of the difference operator and not in the computation of the first derivative. When Dirichlet boundary conditions were imposed, differencing in the exterior direction was performed only on the first application of the difference operator. This convenience eliminates the need for false boundary points and permits direct substitution of either Dirichlet or Neumann data into the difference equations.

The finite volume method has been used to solve Laplace's equation in a region about an ellipse. The grid which was used is shown in Figure 2. A singularity occurs at a vertex of the ellipse where three grid lines intersect at a single point. In order to compare with a known solution, the boundary values of the potential function for ideal flow about an

elliptic cylinder were imposed. Specifically, the boundary value problem

$$\begin{aligned} p_{xx} + p_{yy} &= 0 \text{ in the interior} \\ p_n &= 0 \text{ on the ellipse} \\ p &= x \text{ at the outer boundary} \end{aligned} \quad (10)$$

was solved for the region in Figure 2. Note that only half-cells are depicted at the outer boundary where Dirichlet boundary conditions are imposed at cell centers. The variation of the computed surface potential along the ellipse was in agreement with the theoretical results. However, the solution appeared to be translated by a small constant term. This was traced to a larger than expected error in the coarse grid region near the outer boundary. The error at the outer boundary was subtracted from the numerical solution and the resulting surface potential was compared with the theoretical solution. The absolute error in the surface potential is plotted in Figure 3 beginning with the vertex at  $x=0$  and ending at the vertex  $x=1$  where the singularity occurs. For the number of grid points which were used, one might expect more accurate results. This error was partially due to the large error at the outer boundary which needs further investigation. The computed solution was also not defined on the surface and thus a linear extrapolation of interior values was used to obtain the numerical values which were compared with the actual solution. A further source of error was the fact that the free stream boundary condition was applied only one and a half chord lengths from the ellipse.

The computation of the potential function for flow about the same elliptic cylinder was also carried out using the traditional finite-difference method. Point SOR iterative methods are frequently used for solving elliptic equations on composite grids. That method was used in the above finite-volume calculations and could also be used here. However, it was decided instead to use an ADI method. This example illustrates the special treatment needed at singular points and the successful application of implicit updating along boundary curves in rectangular subregions. In this case there is only one computational rectangle, but there are two re-entrant boundary segments which map to the same interior grid line.

Laplace's equation, as well as other elliptic equations, can be transformed to computational variables and written in the form

$$a p_{\xi\xi} + b p_{\xi\eta} + c p_{\eta\eta} + d p_{\xi} + e p_{\eta} = 0 \quad (11)$$

The ADI method which was used to solve this equation is the Douglas-Rachford algorithm which, after derivatives are replaced by differences, can be written as

$$r_1 p^* - c p_{\eta\eta}^* - e p_{\eta}^* = r_1 p^{(i)} + a p_{\xi\xi}^{(i)} + b p_{\xi\eta}^{(i)} + d p_{\xi}^{(i)} \quad (12)$$

$$r_1 p^{(i+1)} - a p_{\xi\xi}^{(i+1)} - d p_{\xi}^{(i+1)} = r_1 p^* - a p_{\xi\xi}^{(i)} - d p_{\xi}^{(i)} \quad (13)$$

Of course these equations were appropriately modified at the boundary to reflect the Neumann boundary conditions in (10). Suppose that the computational region is the unit square with the image of the ellipse lying along the  $\xi=0$  coordinate line. The grid is similar to Figure 2. Since Dirichlet boundary conditions are imposed at grid points, no half cells are used at the outer boundary. The computations in (12) and (13) can be carried out in the following steps:

- (i) Calculate  $p^*$  on the ellipse.
- (ii) Using the value of  $p^*$  at the singular point, calculate  $p^*$  on the re-entrant segment of the  $\xi=0$  coordinate line.
- (iii) Calculate  $p^*$  on the remaining  $\xi$ -constant coordinate lines.
- (iv) Calculate  $p^{(i+1)}$  on all  $\eta$ -constant coordinate lines which intersect the ellipse at any point other than the singular point.
- (v) Calculate  $p^{(i+1)}$  on the union of all pairs of  $\eta$ -constant lines which intersect at the same interior point of the re-entrant segment.
- (vi) Using a local coordinate system, the value of  $p^{(i+1)}$  at the singular point is computed explicitly.
- (vii) Calculate the values of  $p^{(i+1)}$  on the two  $\eta$ -constant lines which intersect the singular point.

Several modifications of the usual ADI scheme were necessary due to the re-entrant boundary. A periodic tridiagonal system was solved when carrying out the calculation in (i). The system in (v) contains unknowns on, above, and below the re-entrant cut in the physical region. Therefore, the size of the tridiagonal system in (v) was about twice as large as those in (iv) and (vii). Large tridiagonal systems of this type would be common in the use of ADI schemes on composite grids. The system, in general, could contain unknowns from several different subregions.

In this particular case, all the unknowns of a system lie on  $\eta$ -constant lines. However, the orientation of the coordinate line does change at the cut. In a more general case, some of the unknowns could follow  $\eta$ -constant lines in one subregion and  $\xi$ -constant lines in another subregion. Of course these same concepts would apply to any of the other fractional step algorithms such as approximate factorization and locally one dimensional splitting.

The numerical solution of (10) using the iterative algorithm in (12) and (13) was compared with the exact solution, and the absolute error in the surface potential is plotted in Figure 4. It is interesting to note that there was not a loss in accuracy at the outer boundary. Therefore, the finite-difference solution was not subjected to the same type of translation that was observed with the finite-volume solution. The similarities in the behavior of the numerical solution at the two vertices of the ellipse illustrate the successful incorporation of a local coordinate system at the singularity. There was only a slightly larger error at the singular vertex.

Several interpolation schemes for computing on overlapping grids have already been discussed. The objective now is to compare the accuracy of these schemes. The following example also compares the solutions for overlapping grids with one computed on a composite grid with continuously joined grids. The function

$$u(x, y) = 1 - \frac{\log(x^2 + y^2)}{\log(200)}$$

satisfies Laplace's equation everywhere except at the origin. This function was approximated by solving Laplace's equation on the region covered by the overlapping grid in Figure 5. The exact boundary values were used. Since the interior boundary component was taken to be the unit circle, the solution assumed the value 1 on the interior boundary and decreased to nearly zero at the outer boundary. The maximum absolute error in the numerical solution is contained in Table 1. Since the linear and bilinear interpolation formulas can be applied with a smaller overlap region, the error in using these formulas with a one cell overlap is also included. This problem was also solved on the grid in Figure 6 which has approximately the same size grid cells. The error in that solution is also included in Table 1. All the computed solutions had about the same order of accuracy. The second-order interpolation formulas gave better results in each case, although the difference in the error was minimal when the same overlap was used.

A more interesting comparison arises from the function

$$u(x, y) = \sin \frac{2\pi}{\sqrt{x^2 + y^2}}$$

which is the solution of the Poisson equation:

$$u_{xx} + u_{yy} = \phi(x, y).$$

where  $\phi$  is the appropriate source term. The growth of the higher-order derivatives results in a larger truncation error in this example. The maximum absolute error in the numerical solution for some of the overlap cases in the previous example is listed in Table 2. For this function the quadratic Taylor polynomial gave poorer results than the linear Taylor polynomial. Thus we have a case where the numerical approximation of second-order derivatives was unreliable. The biquadratic interpolation formula, which does not require numerical differentiation, was clearly superior to bilinear interpolation.

All of these results were computed using a point SOR iterative method. The convergence rate was considerably greater with an overlap of two grid cells than with a one grid cell overlap. These results are thus consistent with previously reported observations on the relation between the extent of overlap and the convergence and accuracy of the numerical solution. A slightly faster rate of convergence was also noted when using those interpolation formulas with positive coefficients, namely, linear and bilinear.

The most difficult task in applying overlapping grids is to partition each sub-region grid into three sets; those points where the difference equation is applied, the points where the interpolation formula is used, and any points which are not used in the numerical solution of the problem. The code which was written to compute the examples of this report attempted to automate this procedure as far as possible. In the process several different geometric configurations were considered. The solution of Laplace's equation with values 0 and 1 on different boundary components was computed to test the overlap algorithm. Three of those configurations are included since they are representative of cases where overlapping grids would be appropriate. Figure 7 typifies a body in a channel or tunnel. Figure 8 is representative of problems involving flow about multiple bodies. Figure 9 indicates a case where overlapping grids can be used to avoid the large grid line curvature that would result if a single grid were constructed.

## Conclusions

Most of the currently available algorithms for the numerical solution of partial differential equations can be implemented on composite grid systems. Local coordinate systems may be required at special points where the usual differencing techniques cannot be applied. Finite volume formulations are easier to derive on composite grids, and in principle, may be derived for partial differential equations of all types. When using ADI-type algorithms, the main problem is to arrange the order of the computational steps so that all the unknowns at each level are updated simultaneously. Except when using ADI schemes, the overlapping of grids is an alternative to the more common grid construction procedure where grid lines continue smoothly from one subregion into the next. The accuracy of numerical solutions computed on overlapping grids is dependent on both the interpolation formula and the extent of the overlap. Several interpolation formulas were analyzed. In the solution of model problems, the correct choice of the interpolation formula could reduce the error by a factor of two.

## References

1. P. E. Rubbert and K. D. Lee, Patched Coordinate Systems, in *Numerical Grid Generation* (J. F. Thompson, Ed.), Elsevier/North-Holland, New York, 1982.
2. A. Roberts, Automatic Topology Generation and Generalized B-Spline Mapping, in *Numerical Grid Generation* (J. F. Thompson, Ed.), Elsevier/North-Holland, New York, 1982.
3. G. Starius, Composite Mesh Difference Methods for Elliptic Boundary Value Problems, *Numer. Math.* 28 (1977) 243-258.
4. B. Kreiss, Construction of a Curvilinear Grid, *SIAM J. Sci. Stat. Comput.* 4 (1983) 270-279.
5. E. H. Atta and J. Vadyak, A Grid Interfacing Zonal Algorithm for Three-Dimensional Transonic Flows about Aircraft Configurations, AIAA Paper No. 82-1017, June 1982.
6. J. F. Thompson, General Curvilinear Coordinate Systems, in *Numerical Grid Generation* (J. F. Thompson, Ed.), Elsevier/North-Holland, New York, 1982.
7. E. H. Atta, Component-Adaptive Grid Interfacing, AIAA Paper No. 81-0382, January, 1981.

Interpolation Formula	No. Cells Overlap	Max. Absolute Error
Linear on triangles	1	0.00716
Bilinear	1	0.00295
Linear on triangles	2	0.00303
Bilinear	2	0.00158
Linear Taylor poly.	2	0.00273
Quadratic on tri.	2	0.00200
Biquadratic	2	0.00156
Quadratic Taylor poly.	2	0.00211
Continuously joined subgrids		0.00131

Table 1. Error in the approximation of  $u(x,y) = 1 - \log(x^2 + y^2) / \log(200)$  by solving Laplace's equation.

Interpolation Formula	No. Cells Overlap	Max. Absolute Error
Bilinear	2	0.05515
Linear Taylor poly.	2	0.02614
Biquadratic	2	0.02756
Quadratic Taylor poly.	2	0.03158

Table 2. Error in the approximation of  $u(x,y) = \sin(2\pi/x^2 + y^2)$  by solving Poisson's equation.

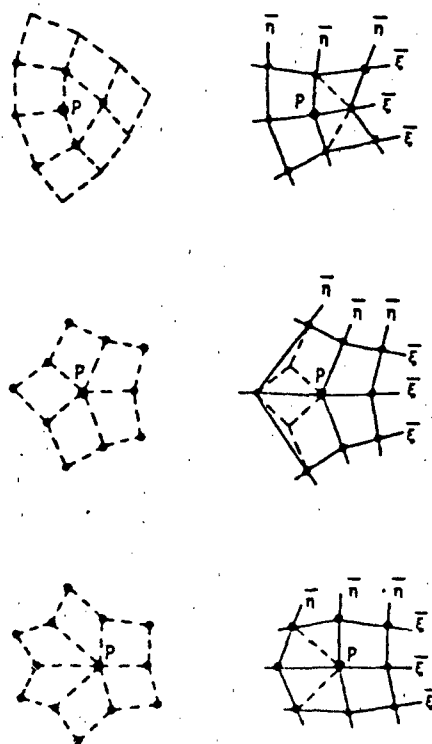


Figure 1. Examples of special points and their corresponding local coordinate systems.

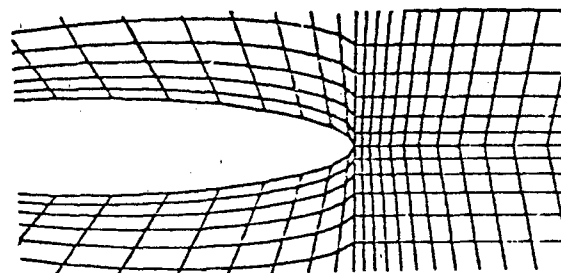
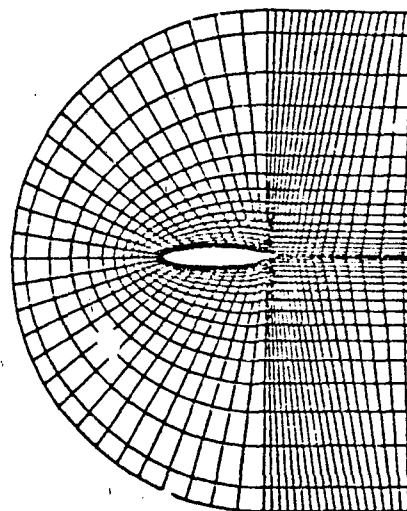


Figure 2. Grid for computing ideal flow about an elliptic cylinder; complete grid and closeup near the singular point.

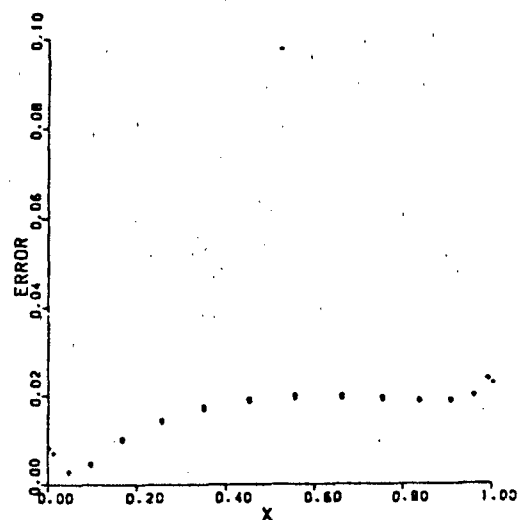


Figure 3. Error in the surface potential computed using the finite-volume method.

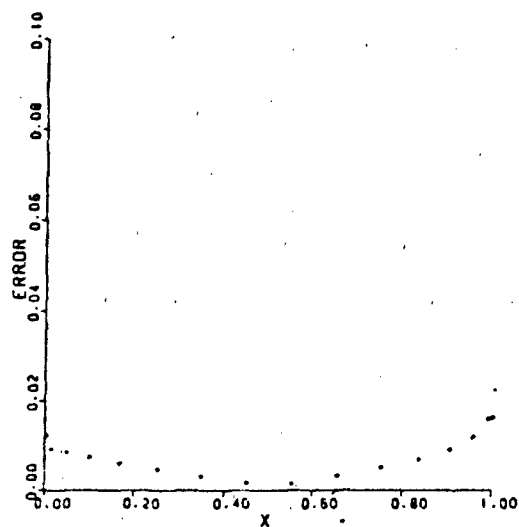


Figure 4. Error in the surface potential computed using the finite-difference method.

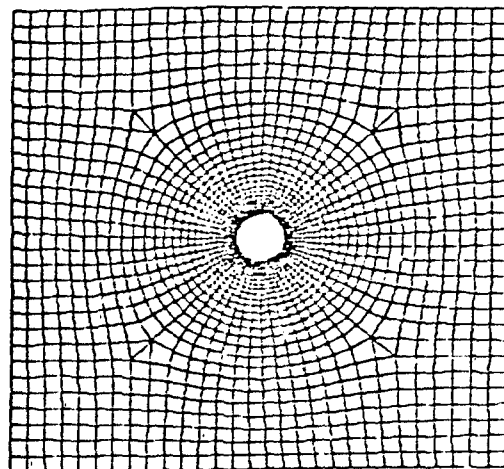


Figure 6. Continuously joined grid.

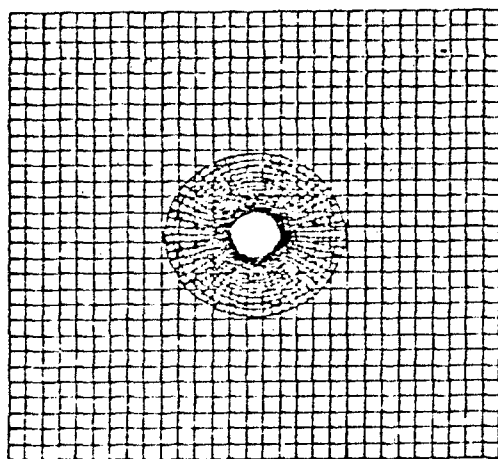


Figure 5. Overlapping grid with an overlap consisting of a two cell wide strip from each subregion.

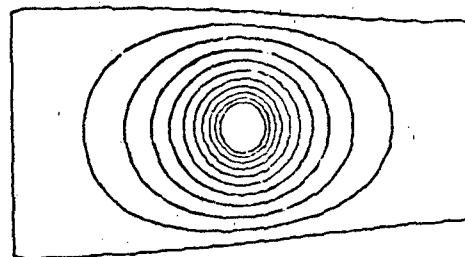
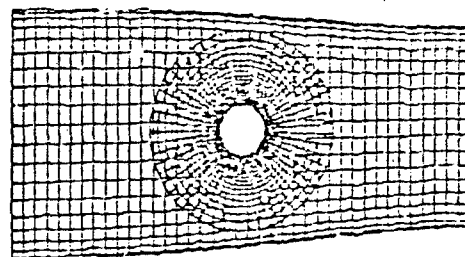


Figure 7. Grid and isotherms for the solution of Laplace's equation with different constant values on the two boundary components.

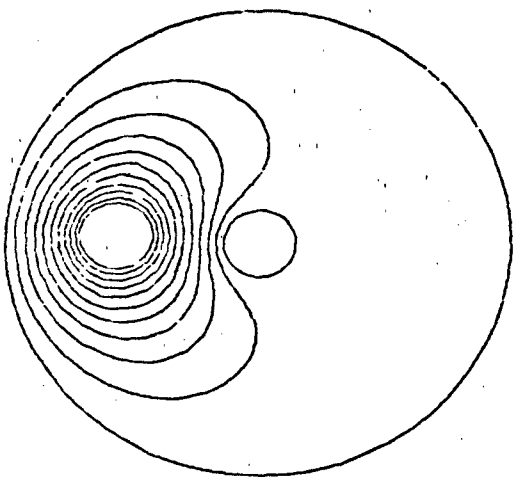
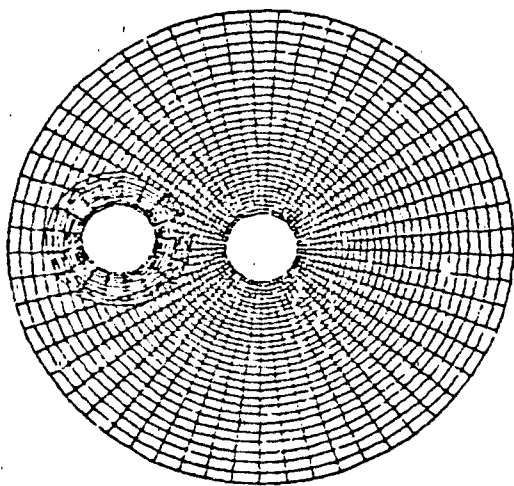


Figure 8. Grid and isotherms for the solution of Laplace's equation with one constant value on the circles with common center and another constant value on the other circle.

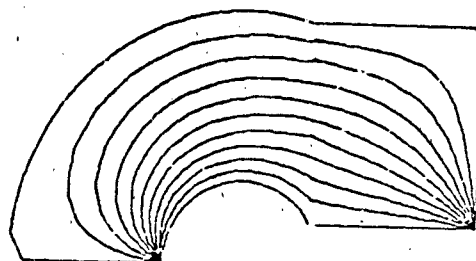
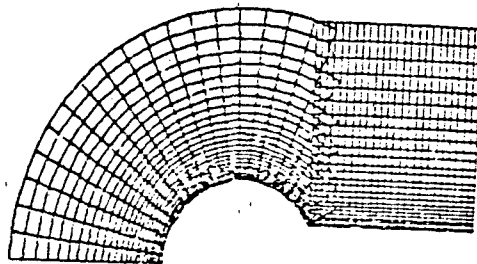


Figure 9. Grid and isotherms for the solution of Laplace's equation with two different constant values on the boundary.

APPENDIX 2

Reference 3

Numerical Grid Generation: Foundations and Applications

"Numerical Implementation"

---relevant excerpt from Chapter IV---

by

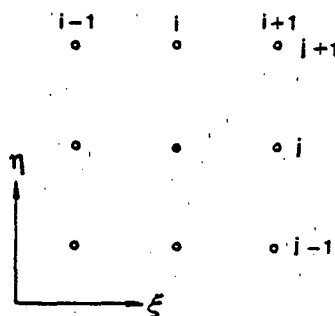
J.F. Thompson, Z.U.A. Warsi, C.W. Mastin

this section by

H.V. McConnaughey

## 2. Discrete Representation of Derivatives

Approximate values of the spatial derivatives of a function which appear in the transformed equations may be found at a given point in terms of the function's value at that point and at neighboring points. As noted earlier, with the problem in the transformed space, only uniform square grids need be considered, hence the standard forms for difference representation of derivatives may be used. For example, in two dimensions the first, second, and mixed partials with respect to the curvilinear coordinates  $\xi$  and  $\eta$  are ordinarily represented at an interior point  $(i,j)$  by finite differences or finite-volume expressions which contain function values at no more than the nine points shown below.



This centered, nine-point "computational molecule" is usually preferred because of the associated difference representations which are symmetry-preserving and second-order accurate. Examples of finite-difference approximations of this type are:

$$(f_{\xi})_{ij} = \frac{1}{2}(f_{i+1,j} - f_{i-1,j}) \quad (11a)$$

$$(f_{\eta})_{ij} = \frac{1}{2}(f_{i,j+1} - f_{i,j-1}) \quad (11b)$$

$$(f_{\xi\xi})_{ij} = f_{i+1,j} - 2f_{ij} + f_{i-1,j} \quad (12a)$$

$$(f_{\eta\eta})_{ij} = f_{i,j+1} - 2f_{ij} + f_{i,j-1} \quad (12b)$$

$$(f_{\xi\eta})_{ij} = \frac{1}{4}(f_{i+1,j+1} - f_{i+1,j-1} - f_{i-1,j+1} + f_{i-1,j-1}) \quad (13)$$

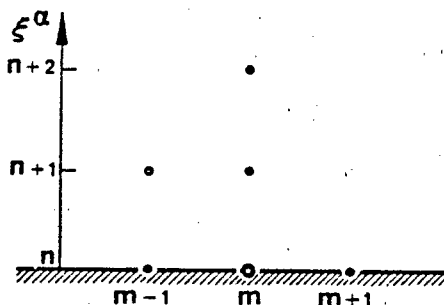
Other second-order approximations of the mixed partial  $(f_{\xi\eta})_{ij}$  which use the nine-point molecule are:

$$\begin{aligned} & \frac{1}{2}(f_{i+1,j+1} - f_{i+1,j} - f_{i,j+1} + 2f_{ij} \\ & - f_{i,j-1} - f_{i-1,j} + f_{i-1,j-1}) \end{aligned} \quad (14)$$

and

$$\begin{aligned} & \frac{1}{2}(f_{i+1,j} - f_{i+1,j-1} + f_{i,j+1} - 2f_{ij} \\ & + f_{i,j-1} - f_{i-1,j+1} + f_{i-1,j}) \end{aligned} \quad (15)$$

It is clear that at boundary points, where at most first partials must be represented, the computational molecule cannot be centered relative to the direction of the coordinate  $\xi^\alpha$  which is constant on the boundary (see diagram below).



There a one-sided difference must be used to approximate  $f_{\xi^a}$ . The second-order formula appropriate for the boundary point indicated above is

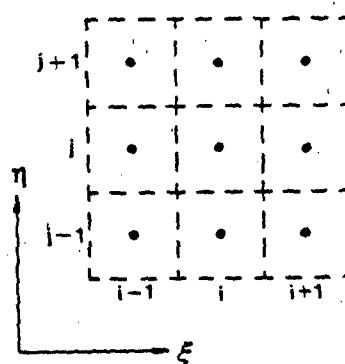
$$(f_{\xi^a})_{mn} = \frac{1}{2}(-f_{m,n+2} + 4f_{m,n+1} - 3f_{m,n})$$

Any standard text on the subject of finite-difference methods will provide formulas of alternate order and/or based on other computational molecules.

A finite-volume approach uses function values at grid-cell centers and approximates derivatives at a cell center by line (surface in 3D) integrals about the cell boundary which are equivalent to averages over the cell. In particular, the identity

$$\nabla f_{\text{avg}} = \frac{1}{V} \int_D \nabla f \, d\tau = \frac{1}{V} \int_{\partial D} f \, \mathbf{n} \, d\sigma \quad (16)$$

is used, where  $V$  is the volume of  $D$ . Thus, if a function is assumed constant along a grid-cell face, it is a simple matter to evaluate the line integral in (16) when  $D$  is a grid cell in transformed space. In terms of the two-dimensional grid:



this approach gives

$$(f_{\xi})_{ij} = f_{i+\frac{1}{2},j} - f_{i-\frac{1}{2},j} \quad (17a)$$

$$(f_{\eta})_{ij} = f_{i,j+\frac{1}{2}} - f_{i,j-\frac{1}{2}} \quad (17b)$$

With an edge value approximated as the average of the center values of the two cells sharing that face, e.g.

$$f_{i+\frac{1}{2},j} = \frac{1}{2}(f_{i+1,j} + f_{ij}) \quad (18)$$

the values given by (17) are equivalent to ordinary central differences (cf. Eq. (11)) and hence are second-order accurate. The first partials of  $f$  may also be assumed constant along each cell edge in order to derive from (16) the following approximations of second and mixed partials at a cell center:

$$(f_{\xi\xi})_{ij} = (f_{\xi})_{i+\frac{1}{2},j} - (f_{\xi})_{i-\frac{1}{2},j} \quad (19a)$$

$$(f_{\xi\eta})_{ij} = (f_{\xi})_{i,j+\frac{1}{2}} - (f_{\xi})_{i,j-\frac{1}{2}} \quad (19b)$$

$$(f_{\eta\xi})_{ij} = (f_{\eta})_{i+\frac{1}{2},j} - (f_{\eta})_{i-\frac{1}{2},j} \quad (19c)$$

$$(f_{\eta\eta})_{ij} = (f_{\eta})_{i,j+\frac{1}{2}} - (f_{\eta})_{i,j-\frac{1}{2}} \quad (19d)$$

Now, however, the averaging scheme in (18) cannot be used to approximate edge values of the derivatives without going outside the nine-point computational molecule shown above. Instead, a second-order accurate representation can be obtained on the nine-point molecule using a forward (backward)

assignment for the center value of a function and a backward (forward) assignment for the first partial on a given side. There are four possible schemes of this type. One uses

$$f_{i+\frac{1}{2},j} = f_{ij}, \quad f_{i,j+\frac{1}{2}} = f_{ij} \quad (20)$$

to evaluate  $\nabla f(\xi, \eta)$  at all cell centers according to (17), and then uses

$$g_{i-\frac{1}{2},j} = g_{ij}, \quad g_{i,j-\frac{1}{2}} = g_{ij} \quad (\text{where } g = f_\xi \text{ or } f_\eta) \quad (21)$$

to evaluate the second and mixed partials given in (19). This method is equivalent to a finite-difference scheme which approximates first partials by backward differences of the function, and then approximates second and mixed partials by forward differences of the first partials. Consequently, the second derivatives which result are equal to those given in Eq. (12), while the resulting representations of the two mixed partials are unequal and only first-order accurate. If the two mixed partials are averaged, however, the second-order expression (15) is recovered. This is also true of the reverse scheme:

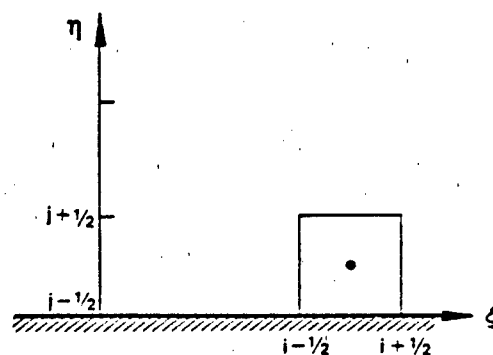
$$f_{i-\frac{1}{2},j} = f_{ij}, \quad f_{i,j-\frac{1}{2}} = f_{ij} \quad (22)$$

$$g_{i+\frac{1}{2},j} = g_{ij}, \quad g_{i,j+\frac{1}{2}} = g_{ij} \quad (g = f_\xi \text{ or } f_\eta) \quad (23)$$

Expressions (12) and (14) are similarly recovered from the other two possibilities (Eq. 20a, 21a, 22b, and 23b or Eq. 20b, 21b, 22a, and 23a). The symmetry-preserving form (13) can be recovered by averaging the averaged mixed partial obtained in one of the first two schemes mentioned and that obtained in one of the remaining two.

The manner in which boundary conditions are treated in a finite volume approach depends on the type of conditions imposed. When Dirichlet conditions are prescribed, it is advantageous to treat the boundary as the center line (plane in three-dimensions) of a row of cells straddling the boundary. The centers of these cells then fall on the physical boundary where the function values are known. When Neumann or mixed conditions are given, however, the boundary is best treated as coincident with cell faces.

Suppose, for example, that boundary condition (9) is to be imposed at the cell edge  $\eta=j-1/2$  indicated below.



The edge value of  $f_{i,j-1/2}$  cannot be approximated by the usual averaging scheme (illustrated by Eq. (18)) since there is no cell center at  $\eta=j-1$ . It can, however, be found in terms of neighboring cell-centered function values by using boundary condition (9) in connection with the forward/backward scheme used to approximate second derivatives at the cell centers.

Considering the scheme represented by Eq. (20) and (21), the values of  $f$  along the cell edges shown above are:

$$f_{i-\frac{1}{2},j} = f_{i-1,j}, \quad f_{i,j+\frac{1}{2}} = f_{ij}$$

$$f_{i+\frac{1}{2},j} = f_{ij}, \quad f_{i,j-\frac{1}{2}} = \text{undetermined} = x_i$$

It follows from Eq. (17) that the first partials of  $f$  at the cell center are

$$(f_\xi)_{ij} = f_{ij} - f_{i-1,j}, \quad (f_\eta)_{ij} = f_{ij} - x_i$$

Eq. (21a,b) then give  $f_\xi$  and  $f_\eta$  along the cell edges enclosing  $(i,j)$  in terms of  $f_{i-1,j}$ ,  $f_{i-1,j+1}$ ,  $f_{ij}$ ,  $f_{i,j+1}$ ,  $f_{i+1,j}$ ,  $x_i$  and  $x_{i+1}$ . In particular,

$$(f_\xi)_{i,j-\frac{1}{2}} = f_{ij} - f_{i-1,j}, \quad (f_\eta)_{i,j-\frac{1}{2}} = f_{ij} - x_i$$

Substitution of these expressions into boundary condition (9) then determines the edge value  $x_i$  as

$$x_i = f_{i,j-\frac{1}{2}} = (\alpha - \beta u \sqrt{g^{22}})^{-1} \cdot \left\{ \gamma - \frac{\beta u}{\sqrt{g^{22}}} [g^{21}(f_{ij} - f_{i-1,j}) + g^{22}f_{ij}] \right\}$$

In this way,  $f$ , and hence  $f_\xi$  and  $f_\eta$ , are found on all boundary-cell edges in terms of cell-centered values of  $f$ .

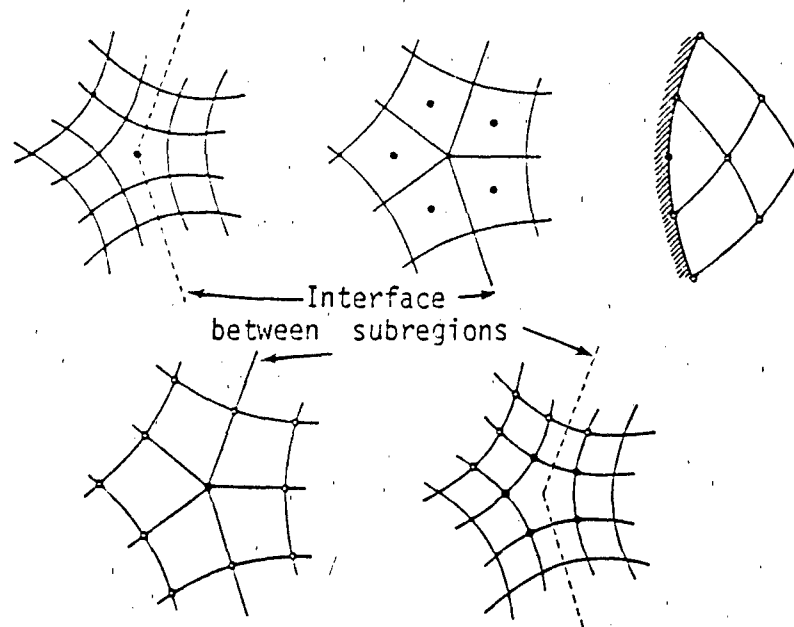
The finite-difference and finite-volume techniques described thus far are appropriate for representing all derivatives with respect to the curvilinear coordinates, even those appearing in the metric quantities. In fact, as it is shown later in this chapter and in chapter V, the metric quantities should be represented numerically even when analytical expressions are available. One might have, for

example,

$$(x_{\xi})_{ijk} = \frac{1}{2}(x_{i+1,j,k} - x_{i-1,j,k}) \quad (24)$$

### 3. Special Points

Many of the expressions given in the previous section break down at so-called "special points" in the field where special attention is required in the approximation of derivatives. These points commonly arise when geometrically complicated physical domains are involved. As indicated in Chapter II, special points can occur on the domain boundary and on interfaces between subregions of a composite curvilinear coordinate system. They may be recognized in physical space as those interior points having a nonstandard number of immediate neighbors or, equivalently, those points which are vertices, or the center, of a cell with either a nonstandard number of faces or a vertex shared by a nonstandard number of other cells. (In two dimensional domains, ordinary interior points have eight immediate neighbors [refer to figure on p. 141]; standard two-dimensional interior grid cells have four sides and share each vertex with three other cells [see diagram on p. 143].) Boundary points are not special unless they are vertex-centered and have a nonstandard number of immediate neighbors (other than five in two dimensions see diagram on p. 142 for an ordinary boundary point) and then are special only when their associated boundary conditions contain spatial derivatives. Some examples of special cell-centered points and special vertex-centered points are shown below.



When a finite-difference formulation is used, the usual approach, as described in Section 2, can be followed at a special point  $P$  if the transformed equations and difference approximations at that point are rephrased in terms of suitable local coordinates. The local system is chosen so as to orient and label only the surrounding points to be used in the needed difference expressions. Choices appropriate to various special points are listed in Tables 1, 2, and 3.

The difficulties encountered at special points in a finite-volume approach are clearly seen by considering the image in the transformed plane. The first pair of diagrams below, for example, shows that at centers of cells having the usual number of faces but sharing a vertex with a non-standard number of cells, such difficulties amount to mere bookkeeping complications when only first partials must be approximated. Equations (17) and (18) still apply, but the indices must be defined to correctly relate the cell centers on the two sides of an interface. The following diagrams

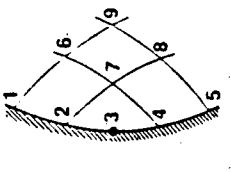
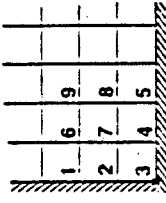
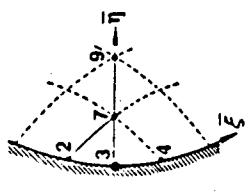
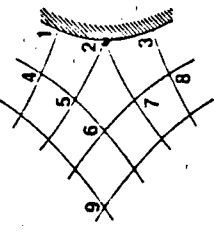
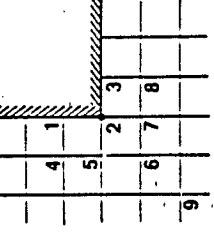
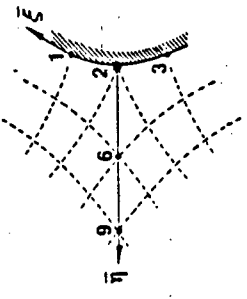
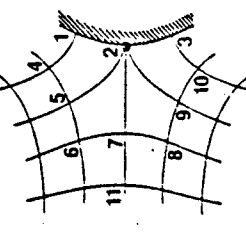
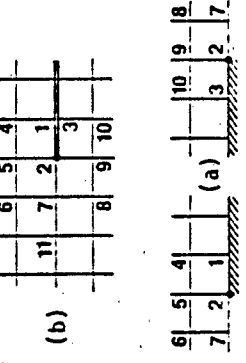
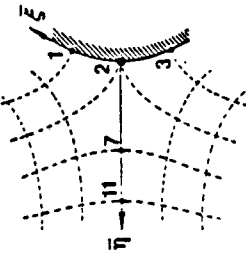
Diagram of special point	Characterization of special point	Image in transformed plane	Local coordinate system
I 	Special point 3 on smooth boundary is transformed to a corner of the computational domain.		
II 	Special point 2 is on an intrusion or interior object and is transformed to a corner of an intruding or interior slab.		
III 	(a) Special point 2 is a branch point on an interior body, or (b) point 2 is on an interior body and is transformed to an end point of a slit.		

Table 1. Special boundary points.

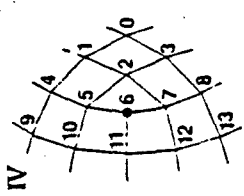
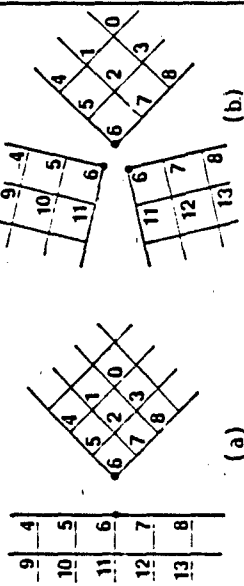
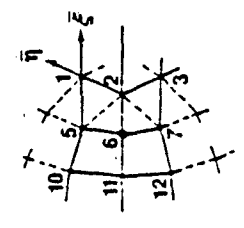
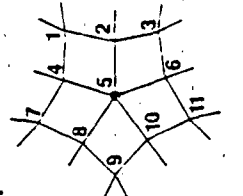
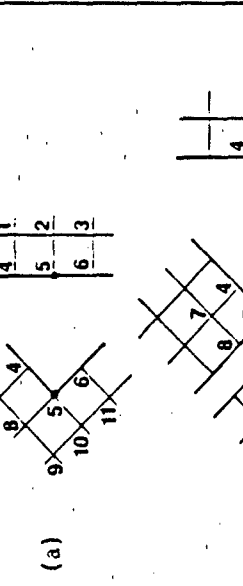
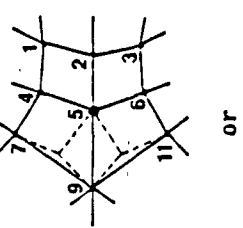
Diagram of special point	Characterization of special point	Image in transformed plane	Local coordinate system
<p>IV</p> 	<p>(a) Special point 6 is common to two subregions. Its image is a corner point for one and an edge point for the other.</p> <p>(b) Special point 6 is common to three subregions. Its image is a corner point for each.</p>		
<p>V</p> 	<p>(a) Special point 5 is common to two subregions. Its image is a concave corner point for one and an edge point for the other.</p> <p>(b) Special point 5 is common to four subregions. Its image is a corner point for three of the segments and an edge point for the fourth.</p> <p>(c) Special point 5 is common to five subregions. Its image is a corner point for each.</p> <p>(d) Special point 5 is common to three subregions. Its image is a corner point for one segment and an edge point for the other two.</p>	 <p>(c) Analogous to IV (b). (d) An obvious modification of V (b).</p>	 <p>or choose points 8 and 10 instead of 7 and 11 if the skewness of segments 9-8 and 9-10 is the same or less than that of segments 9-7 and 9-11.</p>

Table 2. Special vertex-centered interior points associated with subregions joined along grid lines.

Diagram of special point	Characterization of special point	Image in transformed plane	Local coordinate system
VI 	<p>(a) Special point 5 is common to two subregions. It is a branch point in one subregion and an ordinary edge point or the other.</p> <p>(b) Special point 5 is common to two subregions. Its image is an endpoint of a slit in one transformed segment and is an edge point of the other.</p> <p>(c) Special point 5 is common to five subregions. Its image is a corner point for four of the segments and an edge point of the fifth.</p> <p>(d) Special point 5 is common to six subregions. Its image is a corner point for each.</p> <p>(e) Special point 5 is common to four subregions. Its image is a corner point for two of the segments and an edge point for the other two.</p> <p>(f) Special point 5 is common to three subregions and is an edge point for each.</p>	<p>(a) Analogous to V (b).</p> <p>(c) Analogous to IV (b).</p> <p>(e) An obvious modification of VI (e).</p>	<p>or choose points 9 and 11, or 7 and 13, instead of 8 and 12, to obtain the most reasonable system.</p>

Table 2. continued

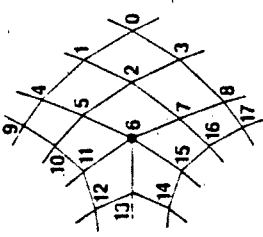
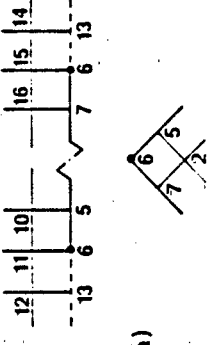
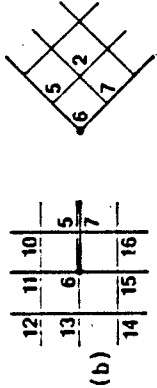
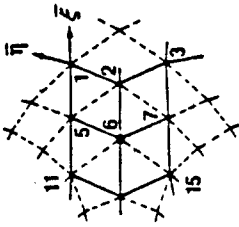
Diagram of special point	Characterization of special point	Image in transformed plane	Local coordinate system
<p>VII</p> 	<p>(a) Special point 6 is common to two subregions. It is a branch point in one subregion and is a corner point in the image of the other.</p> <p>(b) Special point 6 is common to two subregions. Its image is an endpoint of a slit in one transformed segment and is a corner point of the other.</p> <p>(c) Same as V (c).</p> <p>(d) Same as V (b).</p> <p>(e) Same as V (d).</p>	 <p>(a)</p>  <p>(b)</p> <p>(c) Same as V (c).</p> <p>(d) Same as V (b).</p> <p>(e) Same as V (d).</p>	 <p>or choose points 12 and 14, or 10 and 16, instead of 11 and 15, to obtain the most reasonable system.</p>

Table 2. continued

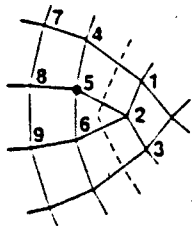
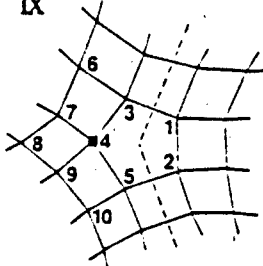
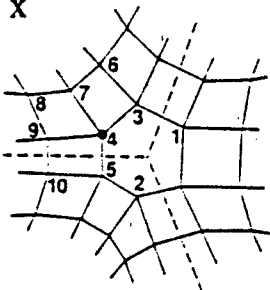
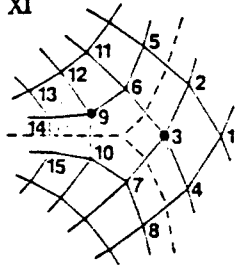
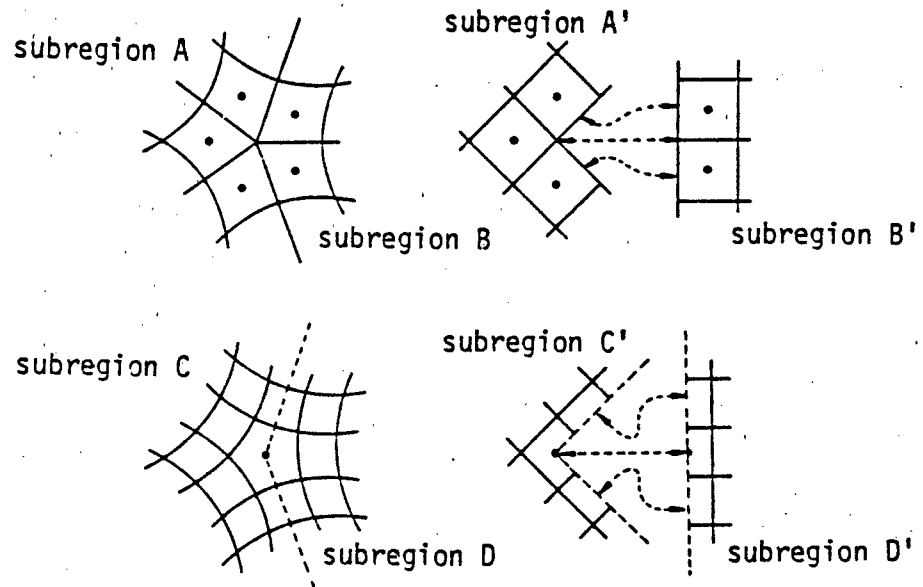
Diagram of special point	Characterization of associated special cell	Point* in local computational molecule
<p>VIII</p> 	<p>Cell center is equivalent to special point 6 in category IV.</p>	<p>(a) Points 1-9, or (b) points 1, 2, 4-6, 8, 9 and use the corresponding antisymmetric, 2nd-order difference for the cross derivative.</p>
<p>IX</p> 	<p>Cell center is equivalent to special point 5 in category V.</p>	<p>(a) Points 3-10 and 1 or 2, or (b) 3-7, 9, 10 and use corresponding antisymmetric, 2nd-order difference for cross derivative.</p>
<p>X</p> 	<p>Cell center is equivalent to special point 5 in category VI.</p>	<p>same as IX.</p>
<p>XI</p> 	<p>Cell center is equivalent to special point 6 in category VII.</p>	<p>(i) At special vertex 3: Use points 1-8 and 9 or 10. (ii) Treat special vertex 9 the same as special vertex 4 in category IX.</p>

Table 3. Special vertex-centered interior points associated with subregions joined between grid lines.

also illustrate the breakdown at all special cell-centered points of the previously-described finite-volume schemes for approximating second and mixed partial derivatives. This is because the forward/backward orientation of the coordinate system in one segment cannot be consistently followed across the interface adjacent to, or intersecting, the special points. The second pair of diagrams displays the additional complication associated with grid cells having a nonstandard number of edges. Such a cell can occur on an interface between segments of a composite grid which are joined between grid lines. When the segments are transformed to their respective images, the separate pieces of the special grid cell cannot be joined without distorting them. It is thus unclear how to evaluate the volume and the outward normals of that transformed cell in order to use identity (16) in the transformed plane. Consequently, at special points of this type and at all special points where second derivatives must be approximated, the governing equations are best represented locally in the physical plane where such ambiguities do not exist.



Treatment in physical space involves approximation of the original equations by means of identity (16). Thus, for a two-dimensional N-sided cell of area A with cartesian centroid  $P = (p_1, p_2)$ , vertices  $V^i = (v_1^i, v_2^i)$   $i=1, 2, \dots, N$ , and edges  $s^i$  joining  $V^i$  and  $V^{i+1}$  ( $V^{N+1} = V^1$ ) along which a function  $f$  and its first partial derivatives are constant, this approach gives

$$f_x^P = A^{-1} \sum_{i=1}^N f^{s^i} (v_2^{i+1} - v_2^i)$$

$$f_y^P = A^{-1} \sum_{i=1}^N f^{s^i} (v_1^i - v_1^{i+1})$$

$$f_{xx}^P = A^{-1} \sum_{i=1}^N f_x^{s^i} (v_2^{i+1} - v_2^i)$$

$$f_{yy}^P = A^{-1} \sum_{i=1}^N f_y^{s^i} (v_1^i - v_1^{i+1})$$

where the superscripts on  $f$  and its derivatives indicate the point or face of evaluation. As in the previous section, an obvious way to approximate  $f^{s^i}$  is to average the center values of the two cells sharing edge  $s^i$ . This same averaging scheme cannot be repeated to approximate  $f_x^{s^i}$ , and  $f_y^{s^i}$ , however, without rejecting the recommended strategy of avoiding use of values at points which are not immediate neighbors of the point at which a quantity is being evaluated. Instead, we propose the averaging technique:

$$f_x^{s^i} = \frac{1}{2} (f_x^{V^i} + f_x^{V^{i+1}})$$

$$f_y^{s^i} = \frac{1}{2} (f_y^{V^i} + f_y^{V^{i+1}})$$

where the vertex values are obtained by applying identity (16) to auxiliary cells formed by joining the midpoints of the edges of each cell to the cell center. To make this more precise, let  $V$  be a vertex common to  $Q$  cells and label the cell faces emanating from  $V$  as  $k^i$  with midpoints

$$M^i = (m_1^i, m_2^i) \quad i=1, 2, \dots, Q.$$

Then if  $P^i = (p_1^i, p_2^i)$  is the center of the cell having edges  $k^i$  and  $k^{i+1}$ , and if

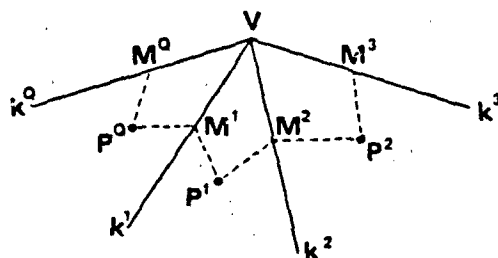
$$f = f^{P^i} \text{ along } M^i P^i \text{ and } P^i M^{i+1}$$

the first partial derivatives of  $f$  at  $V$  may be approximated by

$$f_x^V = A^{-1} \sum_{i=1}^Q f^{P^i} (m_2^{i+1} - m_2^i)$$

$$f_y^V = A^{-1} \sum_{i=1}^Q f^{P^i} (m_1^i - m_1^{i+1})$$

where  $A$  is the area of the  $2Q$ -faced auxiliary cell  $M^1 P^1 M^2 P^2 \dots M^Q P^Q M^1$  indicated in the following diagram.



This technique is applicable to all grid cell centers; however, it is recommended for use only at points where the methods developed in section 2 break down, since the difference representations associated with those methods are simpler.